

Modeling blockage in high directional wireless systems

Evangelos Koutsonas*, Alexandros-Apostolos A. Boulogeorgos*, Stylianos E. Trevlakis[†],
Tanweer Ali[‡], and Theodoros A. Tsiftis^{§¶}

* Department of Electrical and Computer Engineering, University of Western Macedonia, Kozani 50100, Greece.

[†] Research & Development Department, InnoCube P.C., Thessaloniki 55535, Greece.

[‡] Department of Electronics and Communication Engineering, Manipal Institute of Technology,
Manipal Academy of Higher Education, Manipal 576104, India.

[§] Department of Informatics & Telecommunications, University of Thessaly, Lamia 35100, Greece.

[¶] Department of Electrical and Electronic Engineering, University of Nottingham Ningbo China, Ningbo 315100,
China.

Emails: {dece00106, aboulogeorgos}@uowm.gr, trevlakis@innocube.org, tanweer.ali@manipal.edu, tsiftis@uth.gr

Abstract—While the wireless world moves towards higher frequency bands, new challenges arise, due to the inherent characteristics of the transmission links, such as high path and penetration losses. Penetration losses cause blockages that in turn can significantly reduce the signal strength at the receiver. Most published contributions consider a binary blockage stage, i.e. either fully blocked or blockage-free links. However, in realistic scenarios, a link can be partially blocked. Motivated by this, in this paper, we present two low-complexity models that are based on tight approximations and accommodate the impact of partial blockage in high-frequency links. To demonstrate the applicability of the derived framework, we present closed-form expressions for the outage probability for the case in which the distance between the center of the receiver plane and the blocker's shadow center follow uniform distribution. Numerical results verify the derived framework and reveal how the transmission parameters affect blockage.

Index Terms—Blockage, high-frequency communications, modeling, outage probability.

I. INTRODUCTION

As we move towards the next generation wireless systems and networks, the telecommunication traffic in the network is expected to exponentially increase, due to the development of killer-applications, such as extended reality, three-dimensional printing, digital twins, etc., with significant demands on data-rate and inherent security [1]. This creates the need for employing underutilized and non-standardized frequency bands to deal with spectrum scarcity becomes more and more prominent [2]–[4]. As a consequence, the wireless world turned its attention to millimeter wave (mmW), sub-terahertz (THz), THz, and optical bands [5], [6]. However, links that are established in the aforementioned bands suffer from high penetration losses that result in blockages.

Scanning the technical literature, there are several contributions that model and quantify the impact of blockage [7]–[12]. The authors of [7] assumed the obstacles as knife-edge rectangular shapes and categorize them at three categories depending on their dimensions. In the same direction, the

authors of [8] categorized obstacles into four- and two-edge obstacles. In [9], the authors examined the impact of blockage in an indoor wireless network assisted by unmanned aerial vehicles. The authors of [10] studied the effect of human body blockage and introduced a mathematical framework to quantify its impact. The aforementioned contributions focus on obstacle dimensions and their proposed models based on the third-generation partnership project (3GPP) blockage model [13]. All of the presented techniques focus on overcoming the blockage impact, and none of them on understanding its impact on the received signal.

Inspired by the above fact, in [11], the authors employed stochastic geometry to analyze the effect of blockage in indoor THz wireless systems. The analysis of [11] was based on modeling the blockers as cylinders of a randomly chosen position and height, and assuming that the link is either free of blockage or fully blocked. A similar approach was followed in [12], where the authors assumed an exponential random variable to model the probability of establishing a blockage-free link. Again, no partially blocked links were considered.

To cover this research gap, in this paper, we introduce a novel blockage model that accounts for partial blockage. In more detail, we present two low-complexity approximated expressions for the impact of blockage coefficient and we verify their accuracy after analytically comparing them with the exact expressions in terms of mean square error (MSE) and normalized MSE (NMSE). In order to show the applicability of the approximations in complex environments, we present the outage probability of a wireless link that suffer from partial blockage, for the case in which the distance between the center of the receiver plane and the blocker's shadow center follow uniform distribution. The methodology that is adopted for this contribution can be generalized for any distribution of the corresponding distance.

Notations: The absolute value, exponential and natural logarithm functions are respectively denoted by $|\cdot|$, $\exp(\cdot)$, and

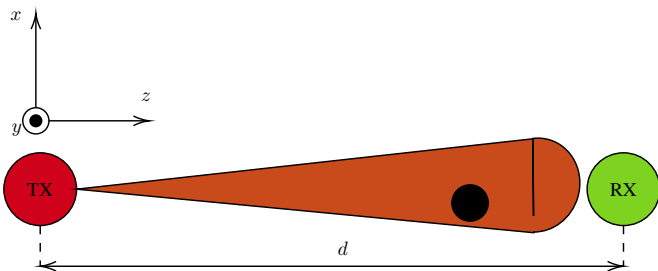


Fig. 1: System model.

$\ln(\cdot)$, \sqrt{x} and $\prod_{l=1}^L x_l$ respectively return the square root of x , and the product of $x_1 x_2 \cdots x_L$. $\Pr(\mathcal{A})$ denotes the probability for the event \mathcal{A} to be valid. The modified Bessel function of the second kind of order n is denoted as $K_n(\cdot)$ [14, eq. (8.407/1)]. The Gamma [14, eq. (8.310)] function is denoted by $\Gamma(\cdot)$, and the error-function is represented by $\text{erf}(\cdot)$ [14, eq. (8.250/1)]. Finally, $G_{p,q}^{m,n} \left(x \left| \begin{matrix} a_1, a_2, \dots, a_p \\ b_1, b_2, \dots, b_q \end{matrix} \right. \right)$ stands for the Meijer G-function [14, eq. (9.301)].

II. BLOCKAGE CHARACTERIZATION

As demonstrated in Fig. 1, we consider a wireless setup that consists of one transmitter (TX), one receiver (RX) and a single obstacle, which is located between the TX and RX. Moreover, we assume that the TX-RX link is highly directional. Note that this is the usual case in high-frequency communications such as millimeter waves (mmW) and terahertz (THz). In this band, the Gaussian TX beam approximation is considered very accurately [15]. Thus, the normalized spatial distribution of the transmitted intensity at distance d from the TX can be obtained as [16]

$$U_b(\boldsymbol{\rho}, d) = \frac{2}{\pi w_d^2} \exp\left(-\frac{2\|\boldsymbol{\rho}\|^2}{w_d^2}\right), \quad (1)$$

where $\boldsymbol{\rho}$ stands for the radial vector from the beam center at distance d . Moreover, w_d represents the beam waste at distance d .

By considering a circular detection aperture of radius α at the RX, we can evaluate the geometric spread as

$$h_b(\mathbf{r}; d) = \int_{\mathcal{A}} U_b(\boldsymbol{\rho}, d) d\boldsymbol{\rho} - \int_{\mathcal{A}_b} U_b(\boldsymbol{\rho} - \mathbf{r}, d) d\boldsymbol{\rho}, \quad (2)$$

where $h_b(\cdot; \cdot)$ represents the fraction of power collected by the RX. Furthermore, \mathcal{A} and \mathcal{A}_b , respectively, stand for the effective areas of RX and the areas shadowed by the blocker at the RX plane.

For tractability, we employ the well-used round-ball approximation for the blocker. In general, when the center of the blocker's shadow at the RX plane is at \mathbf{r} , h_b is a function of $\|\mathbf{r}\|$ as well as the corresponding angle. However, due to the symmetry of the beam and blocker shapes as well as the effective area, $h_b(\mathbf{r}; d)$ depends only on $r = \|\mathbf{r}\|$. Hence, as

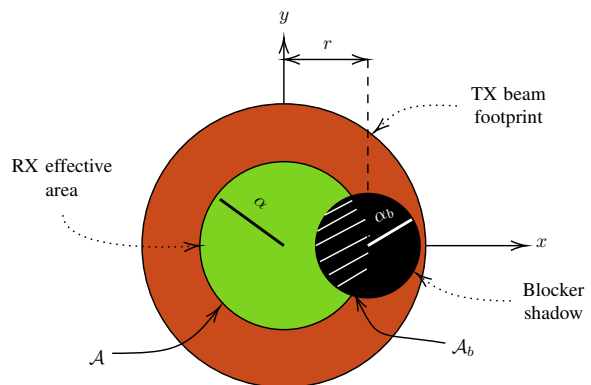


Fig. 2: RX plane.

depicted in Fig. 2, we can assume that the blocker shadow is located along x -axis. Thus, (2) can be rewritten as

$$h_b(\mathbf{r}; d) = \mathcal{I} - \mathcal{I}_b, \quad (3)$$

where

$$\mathcal{I} = \int_{-\alpha}^{\alpha} \int_{-\alpha}^{\alpha} \frac{2}{\pi w_d^2} \exp\left(-2\frac{x^2 + y^2}{w_d^2}\right) dx dy \quad (4)$$

and

$$\mathcal{I}_b = \int_{-\alpha_b}^{\alpha_b} \int_{-\zeta}^{\zeta} \frac{2}{\pi w_d^2} \exp\left(-2\frac{(x-r)^2 + y^2}{w_d^2}\right) dy dx, \quad (5)$$

with

$$\zeta = \sqrt{a_b^2 - x^2}. \quad (6)$$

Moreover, note that in order for the obstacle to influence the portion of reception power, the following inequality should hold:

$$r - a_b < a. \quad (7)$$

After some algebraic manipulations, (4) can be rewritten as

$$\mathcal{I} = \frac{2}{\pi w_d^2} \int_{-\alpha}^{\alpha} \exp\left(-2\frac{y^2}{w_d^2}\right) dy \int_{-\alpha}^{\alpha} \exp\left(-2\frac{x^2}{w_d^2}\right) dx, \quad (8)$$

or equivalently

$$\mathcal{I} = \left(\text{erf}\left(\frac{\sqrt{2}\alpha}{w_d}\right) \right)^2. \quad (9)$$

Similarly, (5) can be rewritten as

$$\mathcal{I}_b = \frac{2}{\pi w_d^2} \int_{-\alpha_b}^{\alpha_b} \exp\left(-2\frac{(x-r)^2}{w_d^2}\right) \mathcal{K}(\zeta) dx, \quad (10)$$

where

$$\mathcal{K}(\zeta) = \int_{-\zeta}^{\zeta} \exp\left(-2\frac{y^2}{w_d^2}\right) dy, \quad (11)$$

which can be rewritten as

$$\mathcal{K}(\zeta) = \sqrt{\frac{\pi}{2}} w_d \text{erf}\left(\frac{\sqrt{2}\zeta}{w_d}\right). \quad (12)$$

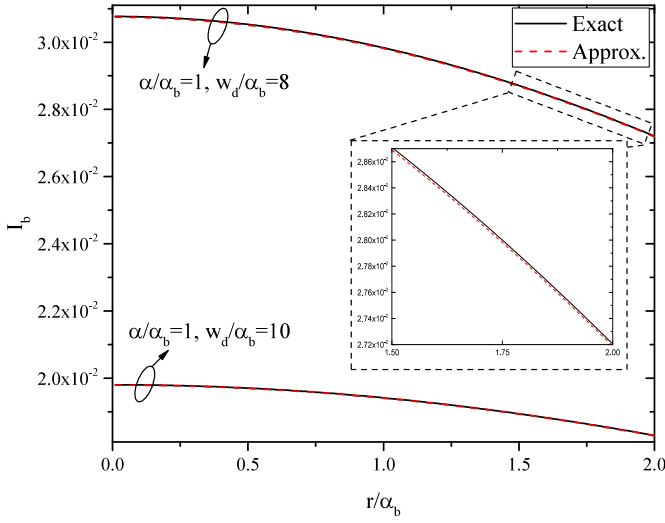


Fig. 3: Exact and approximate values of I_b as a function of r/α_b , for different values of w_d/α_b .

By applying (6) and (12) into (10), we get

$$\mathcal{I}_b = \sqrt{\frac{2}{\pi}} \frac{1}{w_d} \int_{-\alpha_b}^{\alpha_b} \exp\left(-2\frac{(x-r)^2}{w_d^2}\right) \times \operatorname{erf}\left(\frac{\sqrt{2}\sqrt{a_b^2-x^2}}{w_d}\right) dx. \quad (13)$$

Unfortunately, it is very difficult or even impossible to write (13) in a closed form. The following theorems return closed-form tight approximations for I_b .

Proposition 1. A tight closed-form approximation for (10) can be obtained as

$$\mathcal{I}_b \approx \frac{1}{2} \operatorname{erf}\left(\frac{a_b\sqrt{\pi}}{\sqrt{2}w_d}\right) \times \left(\operatorname{erf}\left(\frac{a_b\sqrt{\pi}-2r}{\sqrt{2}w_d}\right) + \operatorname{erf}\left(\frac{a_b\sqrt{\pi}+2r}{\sqrt{2}w_d}\right)\right). \quad (14)$$

Proof: By considering approximation the integration in (5) by an integration over a square of equal area to the obstacle, i.e., with side length $\sqrt{\pi}\alpha_b$, (5) can be approximated as

$$\mathcal{I}_b \approx \frac{2}{\pi w_d^2} \int_{-\frac{\sqrt{\pi}\alpha_b}{2}}^{\frac{\sqrt{\pi}\alpha_b}{2}} \int_{-\frac{\sqrt{\pi}\alpha_b}{2}}^{\frac{\sqrt{\pi}\alpha_b}{2}} \exp\left(-2\frac{(x-r)^2}{w_d^2}\right) \times \exp\left(-2\frac{y^2}{w_d^2}\right) dx dy, \quad (15)$$

which can be written in a closed-form as in (14). This concludes the proof. ■

The approximation presented in Theorem 1, although very tight, does not provide a tractable solution for performance analysis. Motivated by this, the following theorem returns a simplified approximation of I_b .

Proposition 2. A simple closed-form approximation for (13) can be obtained as

$$\mathcal{I}_b \approx C_0 \exp\left(-\frac{2}{w_d^2} \frac{|C_2|}{C_0} r^2\right), \quad (16)$$

where

$$C_0 = \left(\operatorname{erf}\left(\sqrt{\frac{\pi}{2}} \frac{\alpha_b}{w_d}\right)\right)^2 \quad (17)$$

and

$$C_2 = -\sqrt{2} \frac{\alpha_b}{w_d} \operatorname{erf}\left(\sqrt{\frac{\pi}{2}} \frac{\alpha_b}{w_d}\right) \exp\left(-\left(\sqrt{\frac{\pi}{2}} \frac{\alpha_b}{w_d}\right)^2\right). \quad (18)$$

Proof: First, we rewrite (15) as

$$\mathcal{I}_b \approx \frac{2}{\pi w_d^2} \mathcal{J} \int_{-\frac{\sqrt{\pi}\alpha_b}{2}}^{\frac{\sqrt{\pi}\alpha_b}{2}} \exp\left(-2\frac{(x-r)^2}{w_d^2}\right) dx, \quad (19)$$

where

$$\mathcal{J} = \int_{-\frac{\sqrt{\pi}\alpha_b}{2}}^{\frac{\sqrt{\pi}\alpha_b}{2}} \exp\left(-2\frac{y^2}{w_d^2}\right) dy, \quad (20)$$

which can be expressed in closed-form as

$$\mathcal{J} = \sqrt{\frac{\pi}{2}} w_d \operatorname{erf}\left(\sqrt{\frac{\pi}{2}} \frac{\alpha_b}{w_d}\right). \quad (21)$$

By using the Taylor series to extend the exponential term in (19), we get

$$\mathcal{I}_b \approx \frac{2\alpha_b}{w_d} \mathcal{J} + \frac{2}{\sqrt{\pi}} \mathcal{J} \sum_{\substack{k=3 \\ \text{odd}}}^{\infty} \sum_{\substack{l=0 \\ \text{even}}}^k \frac{(-1)^{(k-1)/2}}{k \binom{k-1}{2}!} \times \binom{m}{l} \left(\sqrt{2} \frac{r}{w_d}\right)^l \left(\sqrt{\frac{\pi}{2}} \frac{\alpha_b}{w_d}\right)^{k-l}, \quad (22)$$

which can be rewritten as

$$\mathcal{I}_b \approx \sum_{\substack{l=0 \\ \text{even}}}^{\infty} C_l \left(\frac{\sqrt{2}}{w_d} r\right)^l, \quad (23)$$

where

$$C_l = \frac{2}{\sqrt{\pi}} \mathcal{J} \sum_{\substack{k=l+1 \\ \text{odd}}}^{\infty} \frac{(-1)^{(k-1)/2}}{k \binom{k-1}{2}!} \binom{m}{l} \left(\sqrt{2} \frac{r}{w_d}\right)^l \times \left(\sqrt{\frac{\pi}{2}} \frac{\alpha_b}{w_d}\right)^{k-l}. \quad (24)$$

By equating the first two terms of the Taylor expansion of the Gaussian pulse to the same terms of (23), we get (16). This concludes the proof. ■

Figure 3 demonstrates the precision of the approximation presented in (14). In more detail, the exact and approximate values of I_b are plotted against of r/α_b , for different values of

$$h_b^{(1)}(r; d) \approx \left(\operatorname{erf} \left(\frac{\sqrt{2}\alpha}{w_d} \right) \right)^2 - \frac{1}{2} \operatorname{erf} \left(\frac{a_b \sqrt{\pi}}{\sqrt{2}w_d} \right) \left(\operatorname{erf} \left(\frac{a_b \sqrt{\pi} - 2r}{\sqrt{2}w_d} \right) + \operatorname{erf} \left(\frac{a_b \sqrt{\pi} + 2r}{\sqrt{2}w_d} \right) \right) \quad (25)$$

TABLE I: MSE and NMSE between exact and simplified approximate I_b expressions.

w_d/α_b	MSE	NMSE
2	5.81×10^{-6}	5.99×10^{-5}
3	3.29×10^{-7}	1.52×10^{-5}
4	3.73×10^{-8}	5.25×10^{-6}
5	6.59×10^{-9}	2.25×10^{-6}
6	1.59×10^{-9}	1.11×10^{-6}
7	4.65×10^{-10}	6.07×10^{-7}
8	1.59×10^{-10}	3.59×10^{-7}
9	6.3×10^{-11}	2.25×10^{-7}
10	2.69×10^{-11}	1.49×10^{-7}

w_d/α_b . From this figure, it becomes evident that the maximum approximation error is in the order of 10^{-5} . Similarly, Table I presents the mean square error (MSE) and normalized MSE (NMSE) between the exact and simplified approximations of I_b expressions for different values of w_d/α_b . From this table, we observe that both MSE and NMSE are relatively small; thus, the approximation can be considered to be tight.

Next, applying (9) and (14) to (2), we obtain (25), given at the top of the next page. Moreover, by applying (9) and (16) into (2), we get

$$h_b^{(2)}(r; d) \approx \left(\operatorname{erf} \left(\frac{\sqrt{2}\alpha}{w_d} \right) \right)^2 - C_0 \exp \left(-\frac{2}{w_d^2} \frac{|C_2|}{C_0} r^2 \right). \quad (26)$$

From (26), it becomes evident that

$$0 \leq h_b^{(2)} \leq 1, \quad (27)$$

or equivalently

$$0 \leq \left(\operatorname{erf} \left(\frac{\sqrt{2}\alpha}{w_d} \right) \right)^2 - C_0 \exp \left(-\frac{2}{w_d^2} \frac{|C_2|}{C_0} r^2 \right) \leq 1, \quad (28)$$

which leads to the following inequality

$$A_1 \leq r \leq A_2 \quad (29)$$

where

$$A_1 = \frac{w_d}{\sqrt{2}} \sqrt{\frac{C_0}{|C_2|}} \sqrt{\ln \left(\frac{C_0}{\left(\operatorname{erf} \left(\frac{\sqrt{2}\alpha}{w_d} \right) \right)^2} \right)} \quad (30)$$

and

$$A_2 = \frac{w_d}{\sqrt{2}} \sqrt{\frac{C_0}{|C_2|}} \sqrt{\ln \left(\frac{C_0}{\left(\operatorname{erf} \left(\frac{\sqrt{2}\alpha}{w_d} \right) \right)^2 - 1} \right)}. \quad (31)$$

III. APPLICATIONS

Let us assume that r follows a uniform distribution with probability distribution function (PDF) and cumulative density function (CDF) that can be respectively obtained as in [17]

$$f_r(x) = \begin{cases} \frac{1}{A_2 - A_1}, & \text{for } A_1 \leq x \leq A_2 \\ 0, & \text{otherwise} \end{cases} \quad (32)$$

and

$$F_r(x) = \begin{cases} 0, & \text{for } x < A_1 \\ \frac{1}{A_2 - A_1} (x - A_1) & \text{for } A_1 \leq x \leq A_2 \\ 1, & \text{for } x > A_2 \end{cases} \quad (33)$$

The following proposition returns a closed-form expression for the outage probability of the link, in the case r follows a uniform distribution.

Proposition 1. *If r follows a uniform distribution, the outage probability of the link can be obtained as in (34), given at the top of the next page. In (34), the conditions C_1 , C_2 , and C_3 respectively stand for*

$$C_1 : \frac{w_d}{\sqrt{2}} \sqrt{\frac{C_0}{|C_2|}} \times \sqrt{\ln \left(\frac{1}{C_0} \left(\operatorname{erf} \left(\frac{\sqrt{2}\alpha}{w_d} \right) \right)^2 + \frac{1}{C_0} (\gamma_{\text{th}} - 1) \frac{N_o}{P_s} \right)^{-1}} < A_1, \quad (35)$$

$$C_2 : A_1 \leq \frac{w_d}{\sqrt{2}} \sqrt{\frac{C_0}{|C_2|}} \times \sqrt{\ln \left(\frac{1}{C_0} \left(\operatorname{erf} \left(\frac{\sqrt{2}\alpha}{w_d} \right) \right)^2 + \frac{1}{C_0} (\gamma_{\text{th}} - 1) \frac{N_o}{P_s} \right)^{-1}} \leq A_2 \quad (36)$$

and

$$C_3 : \frac{w_d}{\sqrt{2}} \sqrt{\frac{C_0}{|C_2|}} \times \sqrt{\ln \left(\frac{1}{C_0} \left(\operatorname{erf} \left(\frac{\sqrt{2}\alpha}{w_d} \right) \right)^2 + \frac{1}{C_0} (\gamma_{\text{th}} - 1) \frac{N_o}{P_s} \right)^{-1}} > A_2 \quad (37)$$

Proof: The outage probability is defined as

$$P_o = \Pr(C \leq r_{\text{th}}), \quad (38)$$

$$P_o = \begin{cases} 0, & \text{for } \mathcal{C}_1 \\ \frac{1}{A_2 - A_1} \left(\frac{w_d}{\sqrt{2}} \sqrt{\frac{C_0}{|C_2|}} \sqrt{\ln \left(\frac{1}{C_0} \left(\operatorname{erf} \left(\frac{\sqrt{2}\alpha}{w_d} \right) \right)^2 + \frac{1}{C_0} (\gamma_{\text{th}} - 1) \frac{N_o}{P_s} \right)^{-1}} - A_1 \right) & \text{for } \mathcal{C}_2 \\ 1, & \text{for } \mathcal{C}_3 \end{cases} \quad (34)$$

$$P_o = \Pr \left(r \leq \frac{w_d}{\sqrt{2}} \sqrt{\frac{C_0}{|C_2|}} \sqrt{\ln \left(\frac{1}{C_0} \left(\operatorname{erf} \left(\frac{\sqrt{2}\alpha}{w_d} \right) \right)^2 + \frac{1}{C_0} (\gamma_{\text{th}} - 1) \frac{N_o}{P_s} \right)^{-1}} \right) \quad (47)$$

where C stands for the link capacity and can be obtained as

$$C = \log_2 \left(\frac{h_b P_s}{N_o} + 1 \right), \quad (39)$$

or, after applying (26),

$$C \approx \log_2 \left(\frac{h_b^{(2)} P_s}{N_o} + 1 \right). \quad (40)$$

From (40), (38) can be rewritten as

$$P_o = \Pr \left(\log_2 \left(\frac{h_b^{(2)} P_s}{N_o} + 1 \right) \leq r_{\text{th}} \right), \quad (41)$$

or

$$P_o = \Pr \left(h_b^{(2)} \leq (\gamma_{\text{th}} - 1) \frac{N_o}{P_s} \right), \quad (42)$$

where

$$\gamma_{\text{th}} = 2r_{\text{th}}. \quad (43)$$

Next, we apply (26) in (42) and we obtain

$$\begin{aligned} P_o &= \Pr \left(\left(\operatorname{erf} \left(\frac{\sqrt{2}\alpha}{w_d} \right) \right)^2 - C_0 \exp \left(-\frac{2}{w_d^2} \frac{|C_2|}{C_0} r^2 \right) \right. \\ &\quad \left. \leq (\gamma_{\text{th}} - 1) \frac{N_o}{P_s} \right) \end{aligned} \quad (44)$$

or equivalently

$$\begin{aligned} P_o &= \Pr \left(\exp \left(-\frac{2}{w_d^2} \frac{|C_2|}{C_0} r^2 \right) \right. \\ &\quad \left. \geq \frac{1}{C_0} \left(\operatorname{erf} \left(\frac{\sqrt{2}\alpha}{w_d} \right) \right)^2 + \frac{1}{C_0} (\gamma_{\text{th}} - 1) \frac{N_o}{P_s} \right), \end{aligned} \quad (45)$$

or

$$\begin{aligned} P_o &= \Pr \left(-\frac{2}{w_d^2} \frac{|C_2|}{C_0} r^2 \right. \\ &\quad \left. \geq \ln \left(\frac{1}{C_0} \left(\operatorname{erf} \left(\frac{\sqrt{2}\alpha}{w_d} \right) \right)^2 + \frac{1}{C_0} (\gamma_{\text{th}} - 1) \frac{N_o}{P_s} \right) \right), \end{aligned} \quad (46)$$

or as in (47), given at the top of the next page. From (47), we obtain (48), given at the top of the next page. Finally, by applying (33) in (48), we obtain (34). This concludes the proof. ■

IV. RESULTS & DISCUSSIONS

This section focuses on presenting numerical results, which are verified through simulations, as well as fruitful discussions. The main goal is to extract insights about the probability and severity of the impact of blockage.

In Fig. 4, h_b is presented as a function of r , for different values of f , assuming that $\alpha_b = 1$ cm, $G_r = 30$ dBi, and transmission distance equal to 10 m. Of note, in this result, r is considered deterministic. As expected, for a given f , as r increases, h_b also increases. Moreover, we observe that as f increases, the range of r that affect h_b decreases. For example, for $f = 10$ GHz, h_b is not equal to 1 for r in the range of $[0, 16.05]$ cm, while, for $f = 100$ GHz, h_b is not equal to 1 for r in the range of $[0, 2.5]$ cm. Finally, from this figure, it becomes evident that for the region in which h_b is not equal to 1, the impact of blockage increases as the operation frequency increase. In other words, it becomes apparent that as the frequency increases, the blockage probability decreases, since the transmission beam footprint at the receiver plane decreases, however, the impact of blockage become more severe.

Figure 5 depicts h_b as a function of α_b for different values of r and f . As expected, for given r and f , as α_b increases, the area of the shadow due to blockage increases; thus, h_b decreases. Additionally, for fixed f and α_b , as r increases, the area of the shadow due to blockage decreases; hence, h_b increases. Finally, for given α_b and r , as f increases, the area of the transmission beam footprint at the receiver plane decreases; as a consequence, h_b increases.

V. CONCLUSIONS

In this contribution, we characterized the impact of blockage by presenting a partial blockage. We reported two low-complexity approximated expressions for the impact of blockage coefficient. To highlight the applicability of the approximations in complex environments, we documented the outage probability of a wireless link that suffer from partial blockage, for the case in which the distance between the center of

$$P_o = F_r \left(\frac{w_d}{\sqrt{2}} \sqrt{\frac{C_0}{|C_2|}} \sqrt{\ln \left(\frac{1}{C_0} \left(\operatorname{erf} \left(\frac{\sqrt{2}\alpha}{w_d} \right) \right)^2 + \frac{1}{C_0} (\gamma_{\text{th}} - 1) \frac{N_o}{P_s} \right)^{-1}} \right). \quad (48)$$

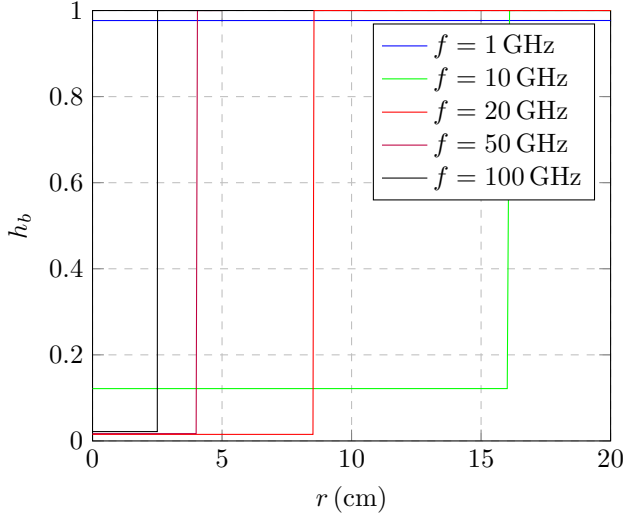


Fig. 4: h_b vs r for different values of f .

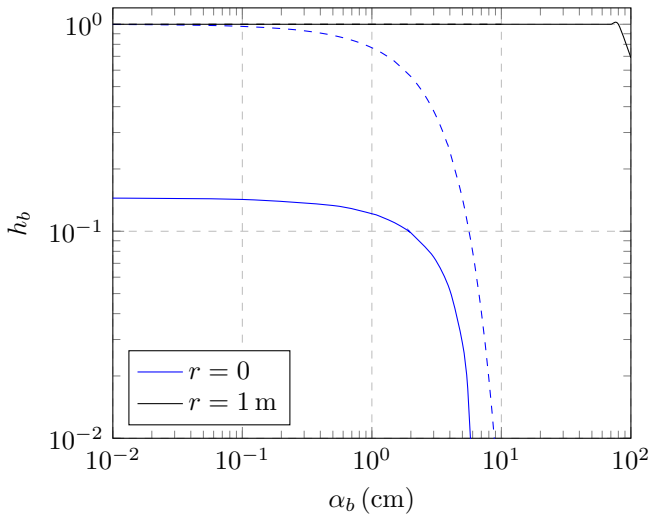


Fig. 5: h_b vs α_b for different values of r and $f = 10$ GHz (dashed lines) and 50 GHz (continuous lines).

the receiver plane and the blocker's shadow center follow uniform distribution. Numerical results verified our finding and revealed the impact of blockage under different setups and transmission parameters.

ACKNOWLEDGMENT

This work was supported by the MINOAS Project within the H.F.R.I call "Basic Research Financing (Horizontal Support of all Sciences)" through the National Recovery and

Resilience Plan "Greece 2.0" funded by the European Union-NextGenerationEU (H.F.R.I.) under Project 15857.

REFERENCES

- [1] D. J. Vergados, A. Michalas, A.-A. A. Boulogeorgos, S. Nikolaou, N. Asimopoulos, and D. D. Vergados, "Adaptive virtual reality streaming: A case for tcp," *IEEE Transactions on Network and Service Management*, vol. 21, no. 2, pp. 1518–1533, 2024.
- [2] A.-A. A. Boulogeorgos, J. M. Jornet, and A. Alexiou, "Directional terahertz communication systems for 6g: Fact check?" *IEEE Vehicular Technology Magazine*, vol. 16, no. 4, pp. 68–77, 2021.
- [3] T. A. Tsiftsis, C. Valagiannopoulos, H. Liu, A.-A. A. Boulogeorgos, and N. I. Miridakis, "Metasurface-coated devices: A new paradigm for energy-efficient and secure 6g communications," *IEEE Vehicular Technology Magazine*, vol. 17, no. 1, pp. 27–36, 2022.
- [4] A.-A. A. Boulogeorgos, S. E. Trelvakis, and N. D. Chatzidiamentis, "Optical wireless communications for in-body and transdermal biomedical applications," *IEEE Communications Magazine*, vol. 59, no. 1, pp. 119–125, 2021.
- [5] A.-A. A. Boulogeorgos, A. Alexiou, T. Merkle, C. Schubert, R. Elschner, A. Katsiotis, P. Stavrianos, D. Kritharidis, P. K. Chartisias, J. Kokkonemi, M. Juntti, J. Lehtomäki, A. Teixeira, and F. Rodrigues, "Terahertz technologies to deliver optical network quality of experience in wireless systems beyond 5G," *IEEE Commun. Mag.*, vol. 56, no. 6, pp. 144–151, Jun. 2018.
- [6] A.-A. A. Boulogeorgos, S. E. Trelvakis, T. A. Tsiftsis, and A. Alexiou, "Toward modeling and assessing the disorientation and misalignment effect in optical wireless nano-networks," *IEEE Journal on Selected Areas in Communications*, vol. 42, no. 8, pp. 2009–2025, 2024.
- [7] S. Kizhakkundil, J. Morais, S. Braam, and R. Litjens, "Four knife-edge diffraction with antenna gain model for generic blockage modelling," *IEEE Wireless Communications Letters*, vol. 10, no. 10, pp. 2106–2109, 2021.
- [8] F. Alsaleem, J. S. Thompson, D. I. Laurenson, S. K. Podilchak, and C. A. Alistarh, "Small-size blockage measurements and modelling for mmwave communications systems," in *2020 IEEE 31st Annual International Symposium on Personal, Indoor and Mobile Radio Communications*, 2020, pp. 1–6.
- [9] W. Tang, J. Y. Dai, M. Z. Chen, K.-K. Wong, X. Li, X. Zhao, S. Jin, Q. Cheng, and T. J. Cui, "MIMO transmission through reconfigurable intelligent surface: System design, analysis, and implementation," *IEEE J. Sel. Areas Commun.*, vol. 38, no. 11, pp. 2683–2699, Nov. 2020.
- [10] M. Gapeyenko, A. Samuylov, M. Gerasimenko, D. Moltchanov, S. Singh, M. R. Akdeniz, E. Aryafar, S. Andreev, N. Himayat, and Y. Koucheryavy, "Spatially-consistent human body blockage modeling: A state generation procedure," *IEEE Transactions on Mobile Computing*, vol. 19, no. 9, pp. 2221–2233, 2020.
- [11] Y. Wu, J. Kokkonemi, C. Han, and M. Juntti, "Interference and coverage analysis for terahertz networks with indoor blockage effects and line-of-sight access point association," *IEEE Transactions on Wireless Communications*, vol. 20, no. 3, pp. 1472–1486, 2021.
- [12] C. Wang and Y. J. Chun, "Stochastic geometric analysis of the terahertz (thz)-mmwave hybrid network with spatial dependence," *IEEE Access*, vol. 11, pp. 25 063–25 076, 2023.
- [13] "Study on channel model for frequencies from 0.5 to 100 ghz (release 18)," 3GPP, Tech. Rep., 2024.
- [14] I. S. Gradshteyn and I. M. Ryzhik, *Table of Integrals, Series, and Products*, 6th ed. New York: Academic, 2000.
- [15] A.-A. A. Boulogeorgos, E. N. Papatotiriou, and A. Alexiou, "Analytical performance assessment of THz wireless systems," *IEEE Access*, vol. 7, no. 1, pp. 1–18, Jan. 2019.
- [16] A. A. Farid and S. Hranilovic, "Outage capacity optimization for free-space optical links with pointing errors," *Journal of Lightwave Technology*, vol. 25, no. 7, pp. 1702–1710, Jul. 2007.

- [17] A. Papoulis and S. Pillai, *Probability, Random Variables, and Stochastic Processes*, ser. McGraw-Hill series in electrical engineering: Communications and signal processing. Tata McGraw-Hill, 2002.